Bulletin of the Seismological Society of America, Vol. 105, No. 3, pp. –, June 2015, doi: 10.1785/0120140263

Ⓔ

The Source of the 30 October 1930 M_w 5.8 Senigallia (Central Italy) Earthquake: A Convergent Solution from Instrumental, Macroseismic, and Geological Data

by Paola Vannoli, Gianfranco Vannucci, Fabrizio Bernardi, Barbara Palombo, and Graziano Ferrari

Abstract On 30 October 1930, an M_w 5.8 earthquake hit the northern Marche coastal area (central Italy), causing significant damage (I_0 VIII–IX degree Mercalli–Cancani–Sieberg) along a 40 km stretch of the Adriatic coast between Pesaro and Ancona, centered on the town of Senigallia. This area is characterized by relatively infrequent and moderate-sized earthquakes and by elusive active faults. In spite of the presence of well-known northwest–southeast-trending, northeast-verging fault-propagation folds forming the outer thrusts of the Apennines, the current level of activity, and the kinematics of these coastal structures are still controversial.

We present a multidisciplinary analysis of the source of the 30 October 1930 Senigallia earthquake, combining instrumental and macroseismic data and elaborations with available evidence from geological and tectonic investigations. We determine the main seismic parameters of the source, including the earthquake location, its magnitude, and, for the first time, its focal mechanism, providing the first instrumental evidence for thrust faulting along the northern Marche coastal belt.

Our findings provide conclusive evidence for the current activity of the northern Marche coastal thrusts. As such they have significant implications for the seismic hazard of the area, a densely populated region that hosts historical heritage, tourism facilities, industrial districts, and key transportation infrastructures.

Online Material: Description of method used for moment tensor computation, tables of focal mechanisms and recording stations, and figures of seismic flux and uncertainty maps for macroseismic epicenters.

Introduction

Damaging earthquakes are often the only means of understanding the tectonics and assessing the seismogenic potential of areas of great geodynamic complexity. Because of its elusive active faults and relatively infrequent earthquakes, Italy is indeed one such area. Reliable source information is generally available for earthquakes of $\mathbf{M} \geq 5.5$ that occurred after the inception of the World-Wide Standardized Seismic Network (WWSSN) in the early 1960s, over 60 yrs after the establishment of the first modern observatories at the end of the nineteenth century; yet many key earthquakes occurred in the early instrumental era (i.e., during those 60 yrs) and were hence recorded by the sparse and heterogeneous seismometers of the time.

Earthquakes of the first half of the twentieth century have been traditionally and rather successfully investigated through their macroseismic signature, that is, based on the distribution of their effects quantified by macroseismic intensity (e.g., Postpischl, 1985; Levret *et al.*, 1994; Bakun and Wentworth, 1997; Gasperini *et al.*, 1999, 2010). More recently, several investigators attempted to derive their essential source parameters, including the earthquake location, magnitude, and focal mechanism, by carefully retrieving, processing, and analyzing all available seismograms (e.g., Baroux *et al.*, 2003, for the 1909 Lambesc earthquake, southern France; Stich *et al.*, 2005, for the 1909 Benavente earthquake, central Portugal; Pino *et al.*, 2008, for the 1930 Irpinia earthquake, southern Italy; Pino *et al.*, 2009, for the 1908 Messina Straits earthquake, southern Italy). In all cases the intensity and instrumentally derived parameters were compared with available tectonic, stress field, and Global Positioning System (GPS) evidence. All in all, the joint analysis of macroseismic, instrumental, and tectonic evidence has turned out to be a promising tool for unveiling the characteristics of these rather elusive earthquakes, providing robust information to

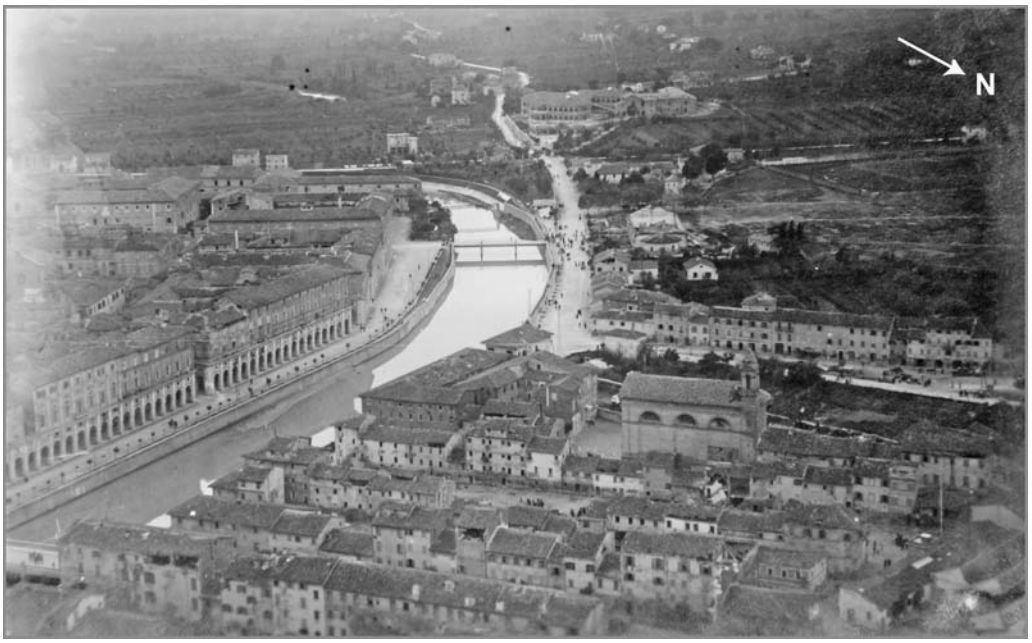

Figure 1. Aerial photo of the Rione Porto (Senigallia). Notice the collapse of roofs and the widespread damage to buildings. The church of Santa Maria del Ponte al Porto and its damaged bell tower is seen in the foreground. The Portici Ercolani are shown on the left side of the image (on the right bank of the Misa River). This rare photo was taken by the air squadrons of the 20th Stormo of the Aeronautica Militare Italiana immediately after the earthquake.

be used for building improved seismogenic models and ultimately for obtaining more reliable seismic-hazard analyses.

In this article, we combined instrumental and macroseismic evidence for the 30 October 1930 Senigallia, central Italy, earthquake (estimated M_w prior to this work: 5.81, I_0 = VIII–IX Mercalli–Cancani–Sieberg [MCS]; see CPTI11 in Data and Resources), with available evidence from geological and tectonic investigations. Positively identifying large active faults and assigning historical earthquakes to each of them is a difficult and often challenging task over much of Italy, and the 1930 earthquake well represents this condition. Difficulties arise from the predominance of blind faulting combined with the presence of the inherited tectonic landscape and with the relatively low rates of present tectonic deformation (see Valensise and Pantosti, 2001a, and Vannoli *et al.*, 2012, 2015, among others).

The 1930 earthquake hit at 07:13:06 UTC, bringing destruction to a large stretch of the northern Marche coastal area between Pesaro and Ancona (Oddone, 1930; Favali *et al.*, 1995; CFTI4Med, see Data and Resources; Figs. 1 and 2). It killed 18 people, injured many more, and caused widespread property damage, leaving hundreds of people homeless. It was felt over a rather large area (inset in Fig. 2), perhaps due to the low attenuation properties at crustal scale of the Adriatic region (Carletti and Gasperini, 2003). The earthquake was followed by a sizeable tsunami ($I = 4$; strong, according to the Sieberg–Ambraseys scale; Pasarić *et al.*, 2012) that flooded the Ancona coastline and was detected by all crews in the city harbor (CFTI4Med, see Data and Resources). Only two direct witnesses are available, from Ancona and from Bakar (A and B, respectively, in the inset of Fig. 2; Pasarić *et al.*, 2012). Therefore, the information on the tsunami is surprisingly limited considering (1) the extent of the Adriatic Sea coasts potentially exposed to it, (2) the distance between the two cities (about 200 km), and (3) that Bakar is located in an embayment protected by the presence of islands parallel to the coast (inset in Fig. 2).

The 30 October 1930 Senigallia earthquake is crucial for a better understanding of the seismic hazard of the northern Adriatic coastal belt. The aim of this article is to improve the knowledge of its source based on the comparison of three end members, namely macroseismic, instrumental, and geological data and elaborations (Table 1).

Seismotectonic Framework

The northern Marche coastal area lies on the eastern side of the Apennines range. The Apennines comprise a typical fold-and-thrust belt that developed in Neogene and Quaternary times at the hanging wall of a west-directed subduction zone. Over time, the Apennines compressional domain migrated toward the northeast as a response to the progressive rollback of the Adriatic lithosphere (e.g., Malinverno and Ryan, 1986). The outer thrusts of the Apennines propagated toward the Adriatic offshore, resulting in a complex pattern of northwest–southeast-trending anticlines and northeast-verging thrust faults and back thrusts running parallel to the coastline (Fig. 3). Because of its significant hydrocarbon potential, the region has been thoroughly investigated using commercial seismic reflection profiles, but the literature offers substantially different interpretations for the architecture of its thrust system. The main differences con-

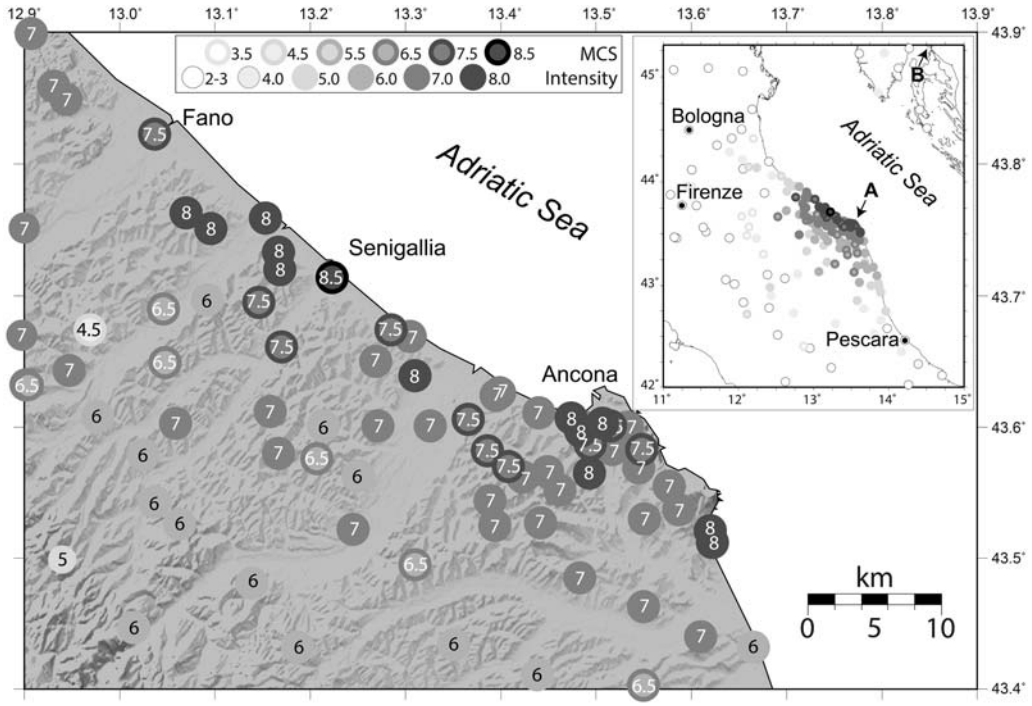

Figure 2. Macroseismic intensities of the 30 October 1930 Senigallia earthquake (CPTI11, see Data and Resources) expressed with the Mercalli–Cancani–Sieberg (MCS) scale (Sieberg, 1931). The inset shows all available intensities. Arrows in the inset show the two localities (A, Ancona; B, Bakar) where the tsunami was observed (CFTI4Med, see Data and Resources; Pasarić *et al.*, 2012).

cern the position of the basal decollement of the thrusts and the presence of secondary shallower decollement levels (thin-skinned versus thick-skinned structural style; e.g., Bally *et al.*, 1986; Barchi *et al.*, 1998). According to the recent work by Maesano *et al.* (2013), the deeper detachment (having a depth of 6–10 km) controls the development of anticlines bounded by major thrust ramps. Overall the tectonic activity of the area is characterized by the interplay of the described thrust faults and a number of east-northeast–west-southwest-trending subvertical faults known as transverse structures (Fig. 3). These exhibit relatively unclear kinematics but are likely to represent regional-scale tear faults that accommodate strain between different portions of the thrust system (Kastelic *et al.*, 2013).

In spite of this relatively clear tectonic framework, the current state of activity and the kinematics of the coastal tectonic structures that may be responsible for the 1930 earthquake and for other events that occurred between Rimini and Ancona is still controversial. Based on the presumed lack of evidence for compressional deformation in post-Early Pleistocene offshore deposits, different investigators suggested that thrusting and folding ended in the Early Pleistocene (Coward *et al.*, 1999; Di Bucci and Mazzoli, 2002) and that current activity is dominated by extensional or strike-slip faulting (Macchiavelli *et al.*, 2012; Mazzoli *et al.*, 2014). Based on geological and geomorphological evidence and on the ongoing seismicity, other investigators maintained that the coastal folds are growing and therefore that the underlying thrust fronts are still active (Vannoli *et al.*, 2004; Scrocca, 2006; Basili and Barba, 2007). As a result of this interpretation, the blind thrust faults located at the leading edge of the Apennines accretionary prism are considered the main seismogenic sources in the area (seismogenic sources were obtained from the Database of Individual Seismogenic Sources (DISS), version 3.1.1, see Data and Resources; Basili *et al.*, 2008; Fig. 3). A recent reanalysis of seismic lines by Maesano *et al.* (2013) led to the identification of growth strata within youthful units, supporting the activity of the most external thrust fronts and allowing their strain rates to be assessed with great accuracy. Finally, Mazzoli *et al.* (2014) used evidence from an earthquake sequence that occurred off the coast of Numana in June 2013 (max M_w 4.9) to suggest that the area is characterized by the occurrence of active strike-slip faults crosscutting the thrust belt.

Figure 4 shows the seismicity of the study area for the period 1981 to present, taken from a recent instrumental catalog (Gasperini *et al.*, 2012, 2013a,b; Lolli *et al*, 2014). The earthquake record is extended back in time up to A.D. 1005 by the CFTI4Med catalog, the CPTI11 catalog, and the International Seismological Centre (ISC) Bulletin (see Data and Resources). Seismicity occurs dominantly along two subparallel belts striking northwest–southest, one elongated following the Apennines axis and the other straddling the Adriatic coast up to 10–15 km offshore (Fig. 4a). Most large historical earthquakes such as that in 1930 occurred along this belt, whereas the area between the Apennines and the coastline appears almost completely silent.

Table 1
Contributions of Instrumental, Macroseismic and Geological Data to the 1930 Senigallia Source

Parameter	Data Type	Method(s)
Location	I	Analysis of seismograms and bulletins
	M	Analysis of intensity distribution
	G	Analysis of geophysical profiles and, if the source is located on land, of the state of deformation of fluvial and coastal terraces
Magnitude	I	(a) Analysis of seismograms; (b) Estimated from focal mechanism
	M	Analysis of intensity distribution based on the attenuation equation of Pasolini *et al.* (2008)
	G	Calculated using empirical relationships between magnitude and fault size
Depth	I	Fixed in the focal mechanism
	M	Analysis of geographical intensities distribution. The estimate however is not reliable
	G	Analysis of geological sections across the active fault system
Length	I	Undetermined
	M	Calculated from magnitude, according to Wells and Coppersmith (1994)
	G	Analysis of (a) geological sections; (b) the area of warped alluvial and coastal terraces
Width	I	Undetermined
	M	Calculated from magnitude, according to Wells and Coppersmith (1994)
	G	Analysis of (a) geological sections; (b) the area of warped alluvial terraces
Strike	I	From focal mechanism
	M	Calculated from intensity distribution: weighted axial mean of the distribution of the axial orientations of sites with higher intensities
	G	Analysis of (a) strike of anticline; (b) modeling of geological data
Dip	I	From focal mechanism
	M	Undetermined
	G	Analysis of geological sections across the active fault system
Rake	I	From focal mechanism
	M	Undetermined
	G	Inferred from geological structures and seismological context

Summary of the contributions of instrumental (I), macroseismic (M), and geological (G) data, and methods for determining the geometric and kinematics parameters of the source of the 30 October 1930 Senigallia earthquake. Undetermined indicates that the specific parameter cannot be determined with the given method or data.

Focal mechanisms are a robust indicator of coseismic strain and provide information on the local tectonic style. The few solutions available for the Marche coastal area (Pondrelli *et al.*, 2002, 2011; Vannucci and Gasperini, 2003, 2004; Scognamiglio *et al.*, 2009; Vannucci *et al.*, 2010, see Data and Resources; Ⓔ for a complete list and representation of focal mechanisms, see Table S1 in the electronic supplement to this article) delineate an area of dominantly strike-slip faulting about 5 km off the coast between Senigallia and Ancona and a belt undergoing compression running inland, 10–20 km from the coastline. Compressional and strike-slip faulting hence coexist in the study area, as both are coherent with the mean direction of the *P* and *T* axes (Fig. 3). The *P*-axis direction is in agreement with the SH_{max} direction retrieved from stress data (Fig. 4a; Heidbach *et al.*, 2008, see Data and Resources) and is perpendicular to the orientation of the main structural elements (anticlines and thrust fronts). GPS data available for the northern Marche area display a general reduction of horizontal velocities with respect to fixed Eurasia along a northeast–southwest trend, suggesting active compression and shortening perpendicular to the coastline (e.g., Devoti *et al.*, 2011).

In summary, the active tectonics record of the northern Marche coastal region is still rather controversial, and the limited evidence from focal mechanisms, stress *in situ* and GPS data does not allow firm constraints to be placed on one tectonic scenario or the other. All of these reasons make investigating the source of the 1930 earthquake a crucial step toward a full understanding of the local tectonic framework and of a careful assessment of the associated earthquake potential.

Identification of the Seismogenic Source

From Geological and Tectonic Data

The source of the 1930 earthquake has been investigated since the early stages of the compilation of the DISS database (see Data and Resources; Valensise and Pantosti, 2001b), as well as in the framework of a specific multidisciplinary investigation of the seismic hazard and seismic response of the town of Senigallia and its surroundings (Mucciarelli and Tiberi, 2007). The hypotheses put forward in the DISS database are based on the observation of active growth of the coastal anticlines of the northern Marche coast. The proposed source, referred to here as the geological source (GS), corresponds with a blind thrust fault (Fig. 3) detected by geophysical prospecting (e.g., Bally *et al.*, 1986; Fantoni and Franciosi, 2010) and causing a distinct signature in the evolution of the coastal landscape. Vannoli *et al.* (2004) investigated the drainage and coastal system and their associated features (channel migrations and avulsions, raised or warped terraces, bedding attitude) along the entire northern Marche coastal belt. They analyzed anomalous drainage patterns and deformed Middle–Late Pleistocene alluvial and coastal ter-

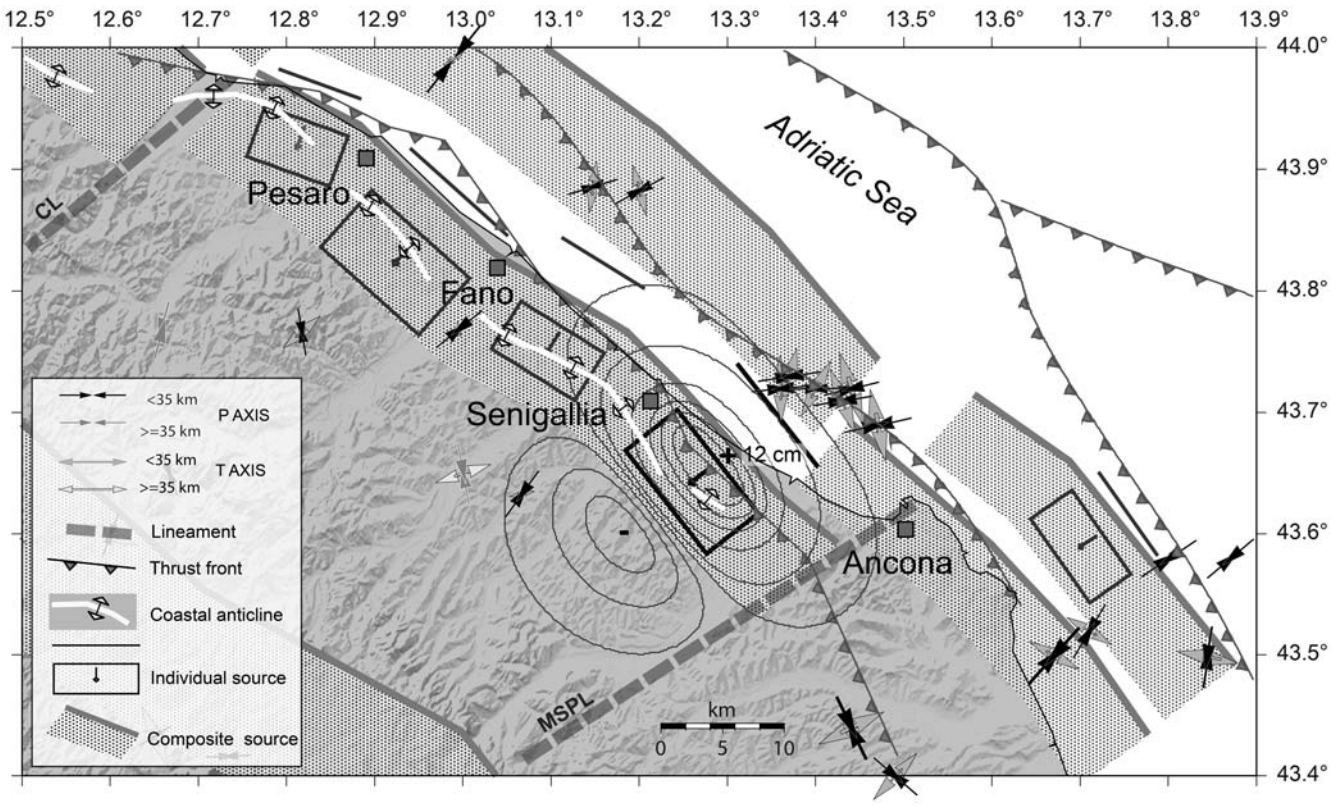

Figure 3. Geological sketch of the study area showing composite seismogenic sources (shown by gray dotted areas) and the individual seismogenic source (Senigallia geological source [GS] is shown by the black individual source) from the Database of Individual Seismogenic Sources (DISS; see Data and Resources) and selected structural elements (Bigi *et al.*, 1992, modified). Ⓔ Depth and orientation of *P* and *T* axes from Vannucci and Gasperini (2003, 2004) are given in Table S1 of the electronic supplement to this article. Contours show the zone of expected uplift (+12 cm of maximum uplift) and subsidence based on the Okada (1985) elastic dislocation code. CL, Conca Line (Elmi *et al.*, 1987); MSPL, Monte San Vicino–Polverigi Line (a set of northeast–southwest faults that includes the Esino Line; Coltorti and Nanni, 1987).

races, identifying, mapping, and correlating with past sea levels a continuous sequence of alluvial and coastal terraces. They found out that terrace treads are consistently warped, suggesting that to produce a significant vertical displacement of the seafloor and generate the observed tsunami, the fault responsible for the Senigallia earthquake must be very close to the coast or offshore. In fact, the DISS database assumes the entire blind thrust front from Pesaro to Ancona to be an active and potentially seismogenic system (Fig. 3).

In detail, the width (7 km) of the GS is based on evidence from seismic reflection profiles, whereas its length (12 km) is constrained on the basis of major fluctuations of the fold axial plane (Vannoli *et al.*, 2004). Based on empirical relationships (Wells and Coppersmith, 1994), this fault size yields a geological magnitude of M_w 5.9. The fault strike and dip are based on the general trend of mapped surface structures and on subsurface data, respectively. The assigned rake corresponds to pure thrusting, in agreement with the geodynamic considerations described in the previous section. The minimum and maximum depth (4.0 and 7.5 km, respectively) are based on subsurface data. Geomorphic markers and growth strata yield slip rate values of 0.24–0.36 mm/yr (Vannoli *et al.*, 2004) and 0.37–0.52 mm/yr (Maesano *et al.*, 2013), respectively, for the Upper Pleistocene and for the Pliocene–Pleistocene. We qualitatively investigated the surface effects of the GS through standard dislocation modeling of a blind fault embedded in an elastic half-space (Okada, 1985) and found that the expected vertical displacement of the hanging wall (Fig. 3) is consistent with geomorphological evidence and with the generation of a small tsunami.

From the Analysis of Macroseismic Data

Italy is blessed with the existence of mature and especially rich macroseismic databases resulting from the pioneering work of local historical seismologists (CFTI4Med and CPTI11, see Data and Resources). These data have been routinely used to derive reliable source parameters for hundreds of preinstrumental or early instrumental earthquakes, although many open issues remain (e.g., on the determination of focal depth and on the correct location of offshore events).

We used the BOXER code (Gasperini *et al.*, 1999, 2010) to derive the essential parameters of the 1930 earthquake source (location, magnitude, source orientation, and source size) from its macroseismic signature, that is to say, a true macroseismic source (MS). BOXER also supplies estimates of the reliability of such parameters, expressed by formal and empirical uncertainties. The latest release of the code provides

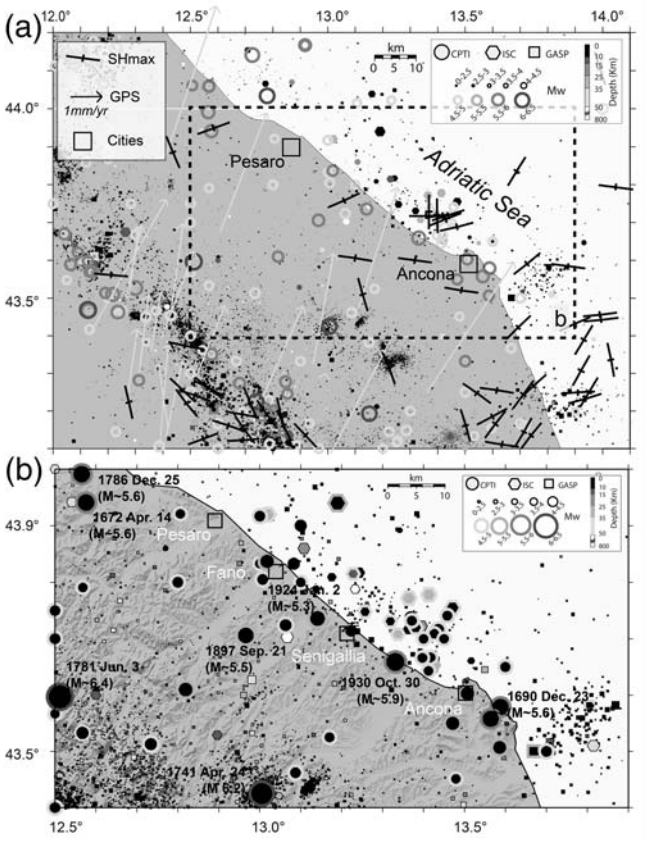

Figure 4. Seismicity and geodynamic characteristics of the region. (a) Orientation of the maximum horizontal compressive stress (Heidbach *et al.*, 2008; see Data and Resources), horizontal Global Positioning System (GPS) velocity vectors (Devoti *et al.*, 2011), and earthquake epicenters from different sources (Villaseñor and Engdahl, 2005; International Seismological Summary [ISS], CPTI11, and International Seismological Centre [ISC], see Data and Resources) for which the M_w was re-evaluated according to the GASP calibration formulas (Gasperini *et al.*, 2012, 2013a,b; Lolli *et al.*, 2014). The legend shows details of catalogs covering different time periods (ISC Bulletin and CPTI11, see Data and Resources); (b) detail of the seismicity.

seven different methods for calculating the macroseismic epicenter (numbered from 0 to 6 in Table 2, Fig. 5, and Ⓔ Fig. S2). Method 0 (barycenter) is based on the area of the largest intensities, whereas methods 1–6 (radiation center) are based on the maximization of the likelihood function of a log–linear extended attenuation equation (Pasolini *et al.*, 2008), with six unknown parameters (epicentral latitude and longitude, hypocentral depth, epicentral intensity, linear and logarithm part of the attenuation equation), using the observed intensity data. Methods 1–6 always estimate the epicenter location (latitude and longitude) and some, by different combinations, or all the other parameters (see Gasperini *et al.*, 2010, for further details). Formal uncertainties are the standard deviation of the parameter averages for method 0, and the variance/covariance matrix for methods 1–6, obtained by inverting the finite-difference Hessian of the likelihood function at its maximum (Guo and Ogata, 1997). Bootstrap simulations (Efron and Tbishirani, 1986; Hall, 1992) allow the empirical uncertainties to be quantified using a variance/covariance matrix and 240 Bootstrap Para-Data (BPDs) sets of the intensity dataset. Very small formal and bootstrap uncertainties reduce the dispersion from the measures and are a robust estimator of the reliability and stability of the parameters obtained.

Figure 5 shows a summary of the macroseismic locations obtained. They are rather distant from each other: locations for methods 0–4 fall onshore within an ~3 km long area, and the associated uncertainties are small, whereas those obtained with methods 5 and 6 fall offshore with relatively large uncertainties (Table 2; Fig. 5). The availability of seven macroseismic epicenters, two of which are located offshore, requires an *a priori* decision on whether the epicenter of the 1930 earthquake has a higher probability of being located inland or offshore. For previous events analyzed by Gasperini *et al.* (2010) and known to have occurred offshore, methods 1–6 have all shown a tendency to shift the epicenter offshore, and all exhibit similar uncertainties. We therefore suggest that most likely the Senigallia earthquake occurred inland. Methods 5 and 6 are the most sensitive to the shifts of the epicenter because the specific calibration of the parameters of the logarithmic and/or linear parts of the attenuation law improves the fit with the entire distribution of the macroseismic data. Hence to fit the distribution of all observed intensities, which is strongly asymmetric due to the presence of the Adriatic Sea and to the lack of data from its opposite (Croatian) shores (Fig. 2), the epicenters tend to shift offshore perpendicular to the coast.

We then used BOXER to compute the macroseismic magnitude, again based on the attenuation equation of Pasolini *et al.* (2008; Table 2, Fig. 5). All methods (0–6) provide similar magnitudes (M_w 5.8 ± 0.1) that are only slightly lower than the M_w obtained by other investigators (e.g., CPTI11, see Data and Resources).

To compute the source ("box") azimuth, BOXER uses a weighted axial mean of the distribution of the axial orientations with respect to the earthquake location, using only the data points where the highest intensities were reported (i.e., the near field of the macroseismic distribution, which includes the localities closest to the seismogenic fault where the ground shaking is greatest due to the physical extent of the rupture). The resulting azimuth (121.4°; Fig. 5) was obtained with method 0; this is the only method that could be used, considering that the alternative epicenters (methods 1–6) are shifted with respect to the highest observed intensities. Although the distribution of intensities is asymmetric due to lack of intensities toward the northeast (i.e., beyond the coastline), BOXER allows a reliable computation of the fault orientation because the epicenter is inland or very close to the coastline. Conversely, when the epicenter is offshore, the source radiation pattern is poorly defined and the source azimuth is indefinite because BOXER expects the intensity data to be more or less evenly distributed. As stated previously, we believe the inland locations supplied by methods 0–4 are reliable. For computing azimuth (method 0) BOXER uses the 13 highest

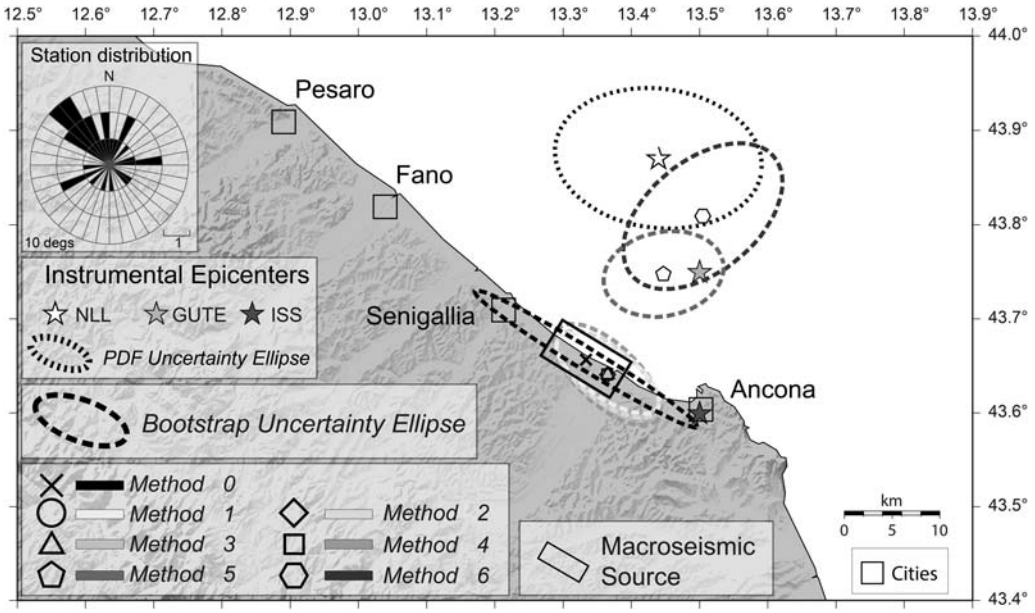

Figure 5. Macroseismic source (MS) and macroseismic epicenters obtained from macroseismic intensities of the 1930 earthquake using all methods made available by the BOXER code (Gasperini *et al.*, 2010; methods 0–6; see the From the Analysis of Macroseismic Data section for further details). The instrumental epicenters made available by the ISS (see Data and Resources), by Gutenberg and Richter (1954; referred to as GUTE), and by this study (NonLinLoc [NLL]) are also shown. Uncertainty ellipses (if shown) are plotted at 90% confidence. A rose diagram indicates the stations for 10° azimuth sectors used for computing the NLL epicenter.

intensities (12 sites with intensity VIII MCS and one with VIII–IX) spread over a relatively large search area.

The stability and reliability of the macroseismic solution for the orientation of the prospective causative fault of the 1930 earthquake is statistically significant because (1) the Rayleigh and Kuiper (Rock, 1988; Fisher, 1993) tests yield <0.1, which implies rejecting the assumption of uniform distribution; (2) the distribution of the frequency of occurrence for all BPDs is very narrow, and there are almost no outliers; and (3) formal (±1.4°) and bootstrap (±4.3°) uncertainties are small. The computed orientation is also roughly similar to the principal axis of the epicentral ellipse uncertainties for methods 0–4 (Fig. 5). Gasperini *et al.* (2010) demonstrated a good correlation between the macroseismic-derived source orientations and the focal mechanisms available for Italian earthquakes, in particular those having $\mathbf{M} \geq 5.7$. By assuming the reliability of their associated statistics, the computed macroseismic orientation has an 80% probability of representing the true strike of the earthquake causative fault, within a confidence range of 10°.

Finally, we combine the macroseismic-derived magnitude and source orientation with the empirical relations of Wells and Coppersmith (1994) to derive a length and a width of 10.2 and 6.4 km, respectively, for the Senigallia MS (Fig. 5).

Earthquake Parameters from the Analysis of Historical Seismograms

Early instrumental estimates of the hypocenter of the 1930 earthquake were supplied by the International Seismo-

Table 2
Macroseismic Parameters Obtained from the Intensity Dataset Using Different Methods Supplied by BOXER

Method	Epicentral Latitude (± bst; ± frm, in km)	Epicentral Longitude (± bst; ± frm, in km)	Offshore/Onshore	M (± bst; ± frm)
0	43.659 (3.818; 4.154)	13.331 (6.173; 6.189)	Onshore	5.80 (0.07; 0.1)
1	43.643 (2.219; 2.29)	13.364 (2.849; 2.286)	Onshore	5.80 (0.02; 0.1)
2	43.642 (2.394; 2.44)	13.363 (2.829; 2.315)	Onshore	5.80 (0.02; 0.1)
3	43.642 (2.441; 2.534)	13.363 (2.808; 2.314)	Onshore	5.80 (0.02; 0.1)
4	43.642 (2.810; 3.278)	13.363 (2.937; 2.321)	Onshore	5.80 (0.02; 0.1)
5	43.750 (2.398; 2.331)	13.446 (3.339; 3.372)	Offshore	5.83 (0.02; 0.1)
6	43.812 (4.061; 4.419)	13.504 (4.414; 4.100)	Offshore	5.85 (0.03; 0.1)

M, magnitude with associated bootstrap (bst) and formal (frm) uncertainties at 90% confidence level (Gasperini *et al.*, 2010). Notice that the magnitude is fairly stable for offshore and onshore solutions.

Table 3
Data and Stations Used for Earthquake Location

Station Code	Latitude (°)	Longitude (°)	Distance (km)	*P* phase	*S* phase	Arrival Time (hh:mm:ss)
VEN	45.433	12.333	195	*P*		07:13:27
VEN	45.433	12.333	195		*SS* (nu)	07:14:04
PAD	45.409	11.886	211	*P*		07:13:27
TRV	45.667	12.183	223	*P*		07:13:28
TRV	45.667	12.183	223		*S* (nu)	07:13:52
RDP	41.758	12.717	242	*P*		07:13:30
RDP	41.758	12.717	242		*SS*	07:14:06
LJU	46.044	14.527	256	*P*		07:13:34
LJU	46.044	14.527	256		*sSS* (nu)	07:14:16
ZAG	45.829	15.994	296	*P*		07:13:39
ZAG	45.829	15.994	296		*sSS*	07:14:22
CSM	40.750	13.900	349	*pP*		07:13:54
CSM	40.750	13.900	349		*S*	07:14:24
GRA	47.077	15.448	389	*P*		07:13:51
GRA	47.077	15.448	389		*SSSS*	07:14:51
BAI	41.107	16.879	417	*Pg* (nu)		07:14:07
BAI	41.107	16.879	417		*SSSS*	07:14:59
ZUR	47.369	8.580	543	*P* (nu)		07:14:04
ZUR	47.369	8.580	543		*S*	07:15:08
MAR	43.305	5.394	651	*pP* (nu)		07:14:27
MAR	43.305	5.394	651		*SS*	07:15:41
CRL	39.133	8.317	678	*pP* (nu)		07:14:30
CRL	39.133	8.317	678		*Sg*	07:15:55
KRL	49.011	8.412	689	*P*		07:14:27
KRL	49.011	8.412	689		*S* (nu)	07:15:45
CHE	50.079	12.376	695	*Pg*		07:14:46
CHE	50.079	12.376	695		*SS* (nu)	07:15:49
JEN	50.952	11.583	800	*P*		07:14:41
JEN	50.952	11.583	800		*S* (nu)	07:16:06
GTT	51.546	9.964	892	*P* (nu)		07:14:50
GTT	51.546	9.964	892		*SS*	07:16:35
DBN	52.102	5.177	1101	*pP* (nu)		07:15:23
DBN	52.102	5.177	1101		*SS*	07:17:24
OXD	51.767	−1.250	1401	*P*		07:15:55
OXD	51.767	−1.250	1401		*SS* (nu)	07:18:32
ALM	36.853	−2.460	1553	*pP*		07:16:21
ALM	36.853	−2.460	1553		*SS*	07:19:04
BID	53.400	−3.067	1604	*P*		07:16:20
BID	53.400	−3.067	1604		*S* (nu)	07:19:06
SEV	44.545	33.668	1610	*P*		07:16:21
CRT	37.190	−3.598	1616	*P*		07:16:21
CRT	37.190	−3.598	1616		*sSS*	07:19:27
SIM	44.949	34.116	1642	*P*		07:16:26
YAL	44.488	34.155	1649	*P*		07:16:24
UPP	59.858	17.627	1800	*P*		07:16:43
UPP	59.858	17.627	1800		*S* (nu)	07:19:46
PUL	59.767	30.317	2101	*P*		07:17:16
PUL	59.767	30.317	2101		*S* (nu)	07:20:41
HLW	29.858	31.342	2218	*P*		07:17:29
HLW	29.858	31.342	2218		*S* (nu)	07:21:11
TNT	43.667	−79.400	7015		*S*	07:31:55
CHK	41.789	−87.599	7669		*S*	07:33:42

Bulletin data: station code and coordinates, epicentral distance, detected *P* and *S* phases (nu = not used), arrival time.

logical Summary (ISS, see Data and Resources) and by Gutenberg and Richter (1954; hereafter referred as GUTE). The ISS hypocenter falls near Ancona, whereas the GUTE hypocenter is located 10 km offshore, between Senigallia and Ancona, at 35 km depth (Fig. 5). The GUTE location, however, is admittedly approximated to the nearest 1/4 of a degree, both in latitude and longitude. The *ISS Bulletin* reports 91 stations for which arrival times are available (64 *P* and 49 *S* phases; Table 3 and Ⓔ Table S2). Neither ISS nor GUTE provides location uncertainties.

The SISMOS project (see Data and Resources) was initiated in 2001 by Istituto Nazionale di Geofisica e Vulcanologia (INGV) scientists. It involves scanning, archiving and distributing historical seismograms, station bulletins, log books, and related information retrieved from Italian and Euro-Mediterranean observatories, and dating as far back as 1895 (Michelini *et al.*, 2005). SISMOS has already retrieved and processed seismograms written by about a thousand strong earthquakes that occurred in the Euro-Mediterranean area from the early 20th century.

For the 30 October 1930 earthquake the SISMOS database supplies 113 high-resolution scans of the seismograms recorded at 34 different stations (Table 4 and Ⓔ Table S2); time corrections for most of these seismograms are not available. The *ISS Bulletin* collects 132 *P* and *S* phases of 90 stations. Therefore, we used the data from the *ISS Bulletin* to locate the earthquake epicenter and a set of historical seismograms to assess its focal mechanism and magnitude.

To relocate the 1930 earthquake and estimate the associated location uncertainty ellipse at 90% confidence (Fig. 5) we used the fully nonlinear earthquake location package NonLinLoc (NLL; Lomax, 2005) with an equal-differential-time (EDT) misfit function. The code performs a probabilistic location of the hypocenter (Fig. 5), quantified by a probability density function (PDF) in a 3D space. The PDF is obtained by means of an equal differential-time formulation of the likelihood function, containing the calculated and observed differences between two stations, summed over all observations pairs. We adopted the ak135 model (Kennett, 2005) for teleseismic phases and a standard Italian crustal model (Basili *et al.*, 1984) for local phases.

The NLL procedure converges to the final solution (longitude, 13.45°; latitude, 43.87°) after five iterations, using 35 phases (21 *P* and 14 *S*) and 29 stations (of the 91 available), with a maximum azimuthal gap of 48° (Table 3; Figs. 5 and 6). This gap increases to about 100° if we take into account only stations located in an area centered on the epicenter and having a radius of 700 km (not considering three stations located about 1600 km away, in Crimea [SEV, SIM, and YAL]; see Fig. 6). Arrival phases were automatically and manually reassociated, and the outliers were eliminated at each iteration. Thanks to the definition of the EDT function (Lomax, 2005), however, the method is not much sensitive to the presence of outliers.

We then computed the focal mechanism and earthquake magnitude by a formal moment tensor (MT) inversion. Because of the instrument response and to the quality of data recording, the procedure used for earthquakes recorded by historical seismographs is significantly different from the procedure used for modern events. More specifically, the MT inversion of old seismograms must face difficulties arising

Table 4
Seismograms Used for Moment Tensor Computation and Associated Instrumental Constants

Station Code	Latitude (°)	Longitude (°)	Distance (km)	It	Comp.	T_0	Damp.	Magn.	Pol	MT
ALI	38.355	−0.487	1316	M	E–W	10	0.28	120		*
ATH	37.972	23.717	1083	M	Z				*	
ATH	37.972	23.717	1083	M	N–S	5.8	0.46	80		*
ATH	37.972	23.717	1083	M	E–W	5.8	0.46	80	*	
CHE	50.079	12.376	695	M	E–W	20	0.53	110	*	*
COP	55.685	12.433	1316	E	E–W	12.7;12.5	0.4;0.4	796		*
DBN	52.102	5.177	1101	E	E–W	25.0;25.0	0.4;0.4	245	*	*
DBN	52.102	5.177	1101	E	N–S	24.4;24.4	0.4;0.4	245	*	
FBR	41.416	2.125	964	M	E–W	9.4	0.42	71		*
FBR	41.416	2.125	964	M	N–S	9.7	0.39	71	*	
HLW	29.858	31.342	2218	M	E–W	12	0.69	250		*
HLW	29.858	31.342	2218	M	Z				*	
JEN	50.952	11.583	800	M	N–S	8.6	0.26	235		*
JEN	50.952	11.583	800	M	E–W				*	
KEW	51.468	−0.313	1329	E	N–S	24.8;25.2	0.4;0.4	880		*
KEW	51.468	−0.313	1329	E	E–W	24.8;25.2	0.4;0.4	880	*	*
PCN	45.050	9.667	327	M	N–S	5	0.5	243	*	
PCN	45.050	9.667	327	M	Z				*	
PCN	45.050	9.667	327	M	E–W	12.5	0.4	2.43	*	
PRA	50.070	14.433	694	M	N–S	9.8	0.5	212	*	
STR	48.579	7.763	682	E	E–W	22.2;22.2	0.4;0.4	460	*	*
UCC	50.798	4.359	1029	E	Z	11.5;8.0	0.4;0.4	880	*	
ZAG	45.829	15.994	296	M	N–S	9	0.37	200	*	
ZAG	45.829	15.994	296	M	E–W	5	0.5	50	*	
ZUR	47.369	8.580	543	M	N–S	5.1	0.33	198	*	
ZUR	47.369	8.580	543	M	E–W	5	0.5	50	*	

Seismogram data: station code and coordinates, epicentral distance, instrument type (It: M, mechanical; E, electromagnetic), instrument component (Comp.), constants (T_0, free period; Damp., damping; Magn., magnification). For electromagnetic instruments, the table supplies the free period and damping of the seismometer and galvanometer, respectively. The last two columns indicate if the seismogram was used for polarity reading (Pol) and/or moment tensor (MT) inversion.

from (1) the static magnification, which in general is significantly smaller than for modern digital broadband seismometers, causing smaller amplitudes and less waveform details; (2) the irregular speed of the seismograph's drum, which introduces velocity phase distortions in the seismograms; (3) fast motion of the seismograph's nib that causes weak or absent traces on the recordings of stations close to the epicenter; (4) the inaccurate synchronization of the station clock used for reading arrival times; and (5) the limited frequency range response and short periods of seismographs (1–20 and 10–30 s for mechanical and electromagnetic instruments, respectively) (Bernardi *et al.*, 2005).

Fifteen stations (Table 4) provided seismograph traces potentially useful for the MT computation of the 1930 event. We used 12 power spectra amplitudes (from 11 stations) and 19 first *P*-phase arrival polarities (from 13 stations) to constrain the *P* and *T* axes. The calculation is based on the method proposed by F. Bernardi *et al.* (unpublished manuscript, 2015; Ⓔ see description in the electronic supplement) and on 5000 synthetic MTs from a Monte Carlo simulation. The method is independent of the location of the epicenter in a range of ∼20 km and allows the MT to be computed also for historical earthquakes, including poorly constrained and highly uncertain ones.

The best-fitting MT solution among all generated synthetic MTs, that is, the solution corresponding to the minimum value of variance, is dominantly compressional but exhibits a minor strike-slip component (strike/dip/rake are 148°/36°/139° and 273°/68°/61°, respectively, for plane 1 and plane 2; Fig. 7). The inferred magnitude is M_w 5.6, to be compared with the M_s 6.0 estimate of the ISS (Villaseñor and Engdahl, 2005, from the Pasadena station) and with the M_s 5.97 (±0.39) estimate supplied by Margottini *et al.* (1993).

Discussion and Conclusions

We characterized the source of the 1930 earthquake by obtaining and comparing a GS, an MS, a standard instrumental relocation, and an MT solution for its magnitude and focal mechanism. The MT solution in particular is a key and original result of this study, based on the processing of pre-WWSSN seismograms with the amplitude spectra method (F. Bernardi *et al.*, unpublished manuscript, 2015; Ⓔ see description in the electronic supplement), and shows a reverse fault with a minor strike-slip component.

First and foremost, the focal mechanism provides new additional constraints on the controversial current state of activity of the northern Marche coastal area. According to this mechanism, a thrust fault is responsible for the occur-

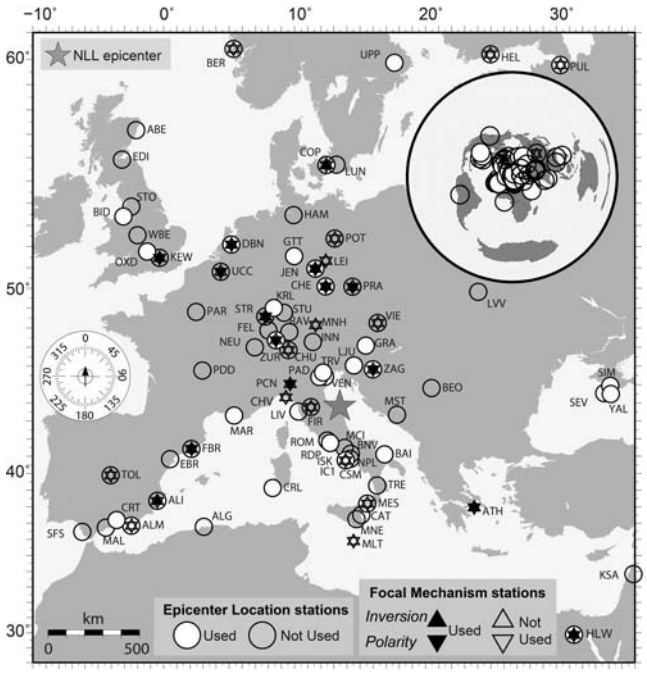

Figure 6. Summary of the stations used (or not used) for locating the 1930 earthquake by NLL (Lomax, 2005) and of the seismograms used (or not used) to assess the focal mechanism by moment tensor (MT) inversion and by analyzing first-motion polarities. The inset indicates the global stations used (or not used) behind the main panel. See Tables 3 and 4 for details on the stations used.

rence of the most significant earthquake that has struck the coastal region between Pesaro and Ancona historically. The new solution is coherent with the observed active compression and thrust kinematics seen along coastal tectonic structures (Vannoli *et al.*, 2004), with the direction of maximum compression axis on the horizontal plane (Heidbach *et al.*, 2008; see Data and Resources) and with GPS velocities (Devoti *et al.*, 2011). No direct evidence is available to choose one of the two nodal planes of the focal mechanism, but most likely the fault responsible for the Senigallia earthquake is one of the relatively large, main northeast-verging thrusts and not a secondary structure related to a southwest-verging back thrust.

The MT method, the geological analysis, and the BOXER code (Gasperini *et al.*, 2010) provided a range of magnitudes (5.6–5.9; Fig. 8) that are in good agreement with previous estimates (CPTI11, see Data and Resources: M_w 5.81; CFTI4Med, M_e 5.8 ± 0.1, see Data and Resources; Margottini *et al.*, 1993, M_s 5.97 ± 0.39). Such fluctuations are well explained by the different data and methods used and also by the different types of magnitude available:

- The solution proposed by Margottini *et al.* (1993) is an M_s obtained from a reappraisal of magnitudes from bulletins.
- The geological magnitude was calculated using an empirical relationship (Kanamori and Anderson, 1975; Wells and Coppersmith, 1994) based on geological evidence. According to Vannoli *et al.* (2004), the observed deformation of the fluvial and coastal terraces is compatible with an ~12 km long fault, yielding M_w 5.9. Being based on long-term geological observations, however, this estimate should be regarded as a maximum.
- The solution obtained from macroseismic observations using the BOXER code is M_w 5.8 ± 0.1. This estimate should be considered equivalent to M_w because the earthquakes used for calibration are events for which an instrumental M_w is available.
- The M_w from MT is directly computed from seismograms after correction for the poles and zeros of the instruments. However, the M_w 5.6 computed from MT is lower than the magnitudes derived from both geological and macroseismic observations. This may be due to the behavior of the mechanical seismometers, which act like a high-pass filter and exhibit very low sensitivity to phases with periods of 20 s or longer. For this reason and because the macroseismic (M_w 5.8 ± 0.1) and the geological (M_w 5.9) magnitudes are consistent with each other, we set our preferred magnitude to M_w 5.8 ± 0.1.

The MT inversion method (F. Bernardi *et al.*, unpublished manuscript, 2015) does not discriminate among all possible hypocentral locations within a radius of ~20 km, implying that the MT solution is compatible with both a blind thrust located close to the coast and with a fault offshore (Fig. 3). Both of these potential sources may generate enough vertical displacement of the seafloor to explain the tsunami observations in Ancona. As for Bakar, we maintain that the account by Pasarić *et al.* (2012) is unreliable and that propagation of the 1930 tsunami across the entire Adriatic Sea is rather unrealistic.

Gasperini *et al.* (2010) tested the correspondence between macroseismic and instrumental epicenters for post-WWSSN earthquakes and found that ~60% agree within 10 km. This implies that the macroseismic location is reliable enough to be confidentially extended in time for older earthquakes. Methods 0–4 locate the epicenter in a narrow area along the coast, whereas only methods 5 and 6 place the epicenter offshore, near the NLL solution (Figs. 3 and 5). As discussed earlier, available oil industry profiles show a large and presumably active fault constrained in the 4.0–7.5 km depth interval below the area indicated by methods 0–4. The joint interpretation of the available evidence suggests that the 1930 earthquake was caused by a fault located inland but very close to the coast (in fact, the coast is believed to be controlled by fault activity), where the GS and MS sources are very close.

The instrumental location calculated with NLL falls ~20 km north of the macroseismic epicenter MS (Fig. 5). This is not surprising in view of the considerable uncertainties affecting instrumental records from the first half of the twentieth century, largely resulting from the sparseness of the available stations and from their large epicentral distance. In addition to the intrinsic limitations of old instrumental data (extensively discussed in F. Bernardi *et al.*, unpublished manuscript, 2015; Ⓔ see description in the electronic supplement), the 1930 earthquake has the disadvantage of a poor azimuthal coverage

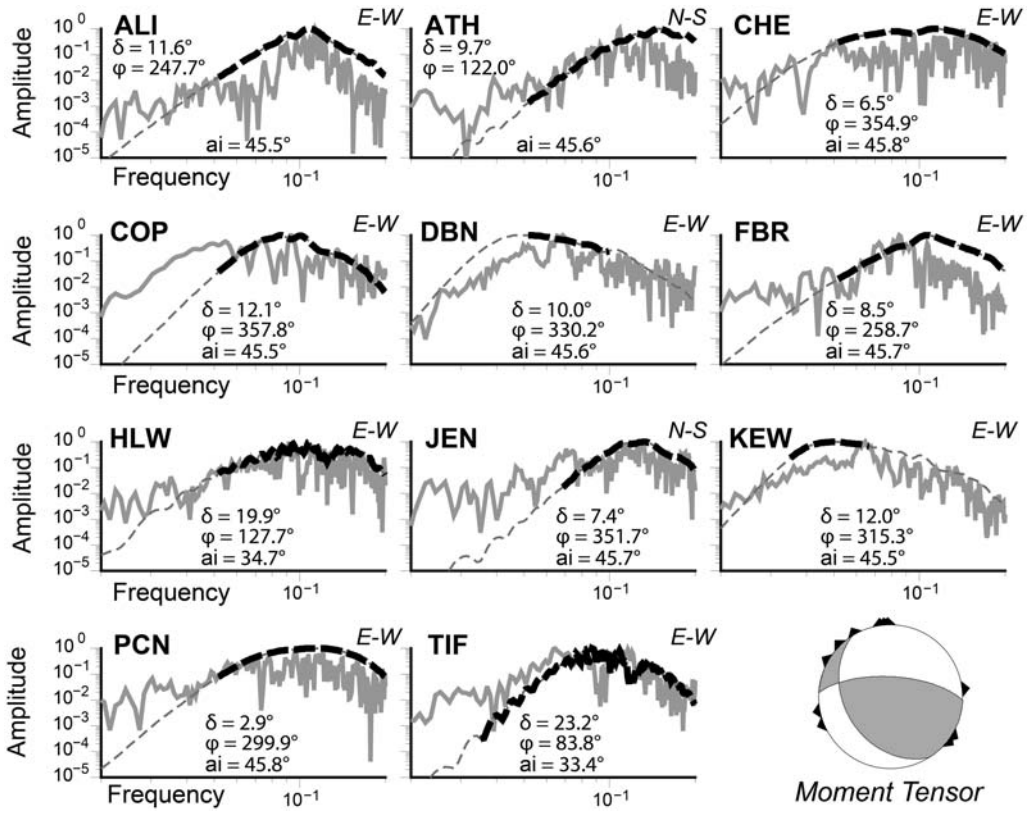

Figure 7. Power spectra amplitudes of the stations used for MT inversion. Station codes, seismogram directions (east–west/north–south), synthetic (dark dashed lines), and observed (gray line) power spectra amplitudes are shown. Distance (δ), azimuth (ϕ), and takeoff angles (ai) between epicenter and stations are also indicated.

of the stations used by NLL, which exhibit a nonhomogeneous distribution with a strong concentration in the northwest quadrant (see rose diagram in Fig. 5). Different location methods yield different instrumental epicenters that are difficult to rank based on their reliability. The bottom line is that, as noted by previous investigators (e.g., Pino *et al.*, 2009), historical instrumental data are crucial for assessing the magnitude and the focal mechanism of significant earthquakes of the pre-WWSSN era, but macroseismic data are generally more robust for determining the earthquake epicenter.

Figure 8 summarizes the geometrical and kinematic parameters of the MT, MS, and GS solutions, highlighting a good correspondence among the orientation of the MT preferred nodal plane (148°), the strike of the GS (142°), and the strike of the MS (121°; Fig. 8). The dip of the selected nodal plane of the MT (36°) is in good agreement with the dip of the thrust fault detected through geophysical prospecting (30°) and subsequently adopted for the GS.

In summary, our results constrain the source of the 1930 earthquake as:

- being located close to the coast,
- at shallow crustal depth (between ~4.0 and ~7.5 km depth),
- striking parallel to the coast,
- dipping to the southwest at ~30°,
- with dominantly thrust faulting kinematics.

The 1930 earthquake was hence caused by a shallow-dipping fault lying beneath one of the northwest–southeast-trending, northeast-verging fault-propagation folds of the Central Apennines thrust belt. This implies that not only the northern Marche coastal thrust fronts are active, as suggested by previous workers, but that they are also seismogenic and are likely to be responsible for all the largest historical earthquakes of the coastal belt. Not coincidentally, the source of the Senigallia earthquake is very similar to that of the 20 and 29 May 2012, Emilia earthquakes (M_w 6.1 and 6.0, respectively; see Anzidei *et al.*, 2012, and papers therein), generated by faults lying beneath the westward prolongation of the same thrust fronts.

Our findings have strong implications for the seismic hazard of the densely populated northern Marche, a coastal region that hosts a number of historical buildings, tourism facilities, industrial districts, and key transportation infrastructures. The 1930 earthquake provides the first instrumental evidence for the activity of the frontal thrusts running beneath the present coastline. Similar-sized thrusts have been identified as potential seismogenic sources by the DISS database v.2.0 (Valensise and Pantosti, 2001b), both northwest and southeast of Senigallia (Fig. 3); two of them in particular, located near Fano and Pesaro, have been described as potential seismic gaps because they appear historically silent. Our findings show that a moderate-sized earthquake (M_w <6.0)

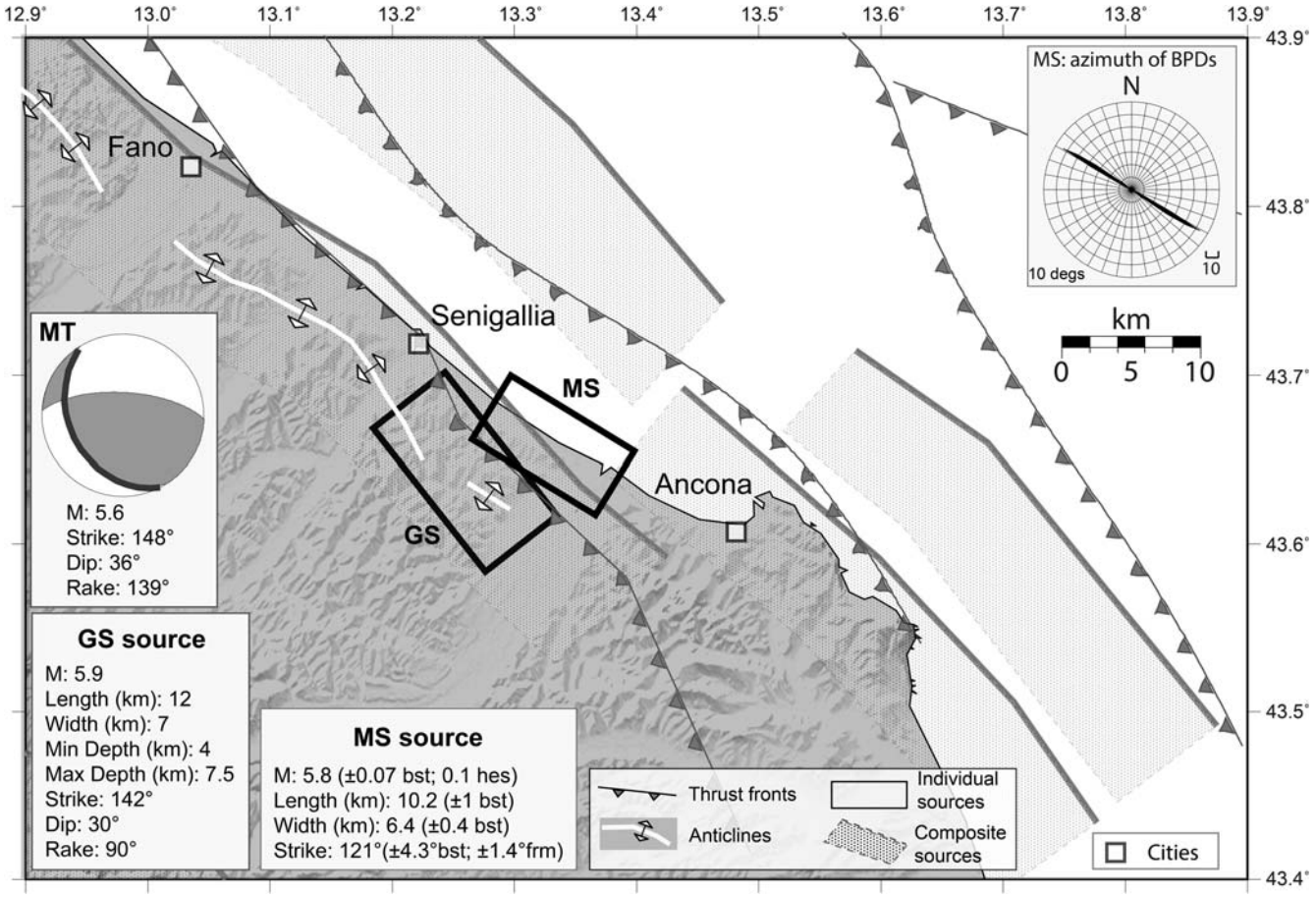

Figure 8. MS and GS parameters for the 1930 earthquake, with geometric and kinematics parameters, compared with the preferred plane (thick black line) resulting from the MT inversion. The rose diagram shows the azimuth distribution of macroseismic Bootstrap Para-Datas. Bootstrap (bst), formal (frm), and hessian (hes) uncertainties (Gasperini *et al.*, 2010) are shown at 90% confidence (see the From the Analysis of Macroseismic Data section for further details).

may represent a major threat for this region, suggesting that these quiescent seismogenic sources should be considered with special care.

Data and Resources

The Database of Individual Seismogenic Sources (DISS), v.3.1.1 was searched using http://diss.rm.ingv.it/diss/ (last accessed July 2014). The Catalogue of Strong Earthquakes in Italy (461 B.C. to 1997) and Mediterranean Area (760 B.C. to 1500) (CFTI4Med) by E. Guidoboni, G. Ferrari, D. Mariotti, A. Comastri, G. Tarabusi, and G. Valensise (2007) was searched using http://storing.ingv.it/cfti4med/ (last accessed July 2014). The *International Seismological Centre Bulletin* (ISC) was searched using www.isc.ac.uk (last accessed December 2013). The International Seismological Summary (ISS) was searched using http://storing.ingv.it/ISS/TIF/i30q4ind.html (last accessed March 2014). The Parametric Catalogue of Italian Earthquakes (CPTI11; doi: 10.6092/INGV.IT-CPTI11) was searched using http://emidius.mi.ingv.it/CPTI (last accessed July 2014). The SISMOS project was searched using http://sismos.ingv.it/en/ (last accessed February 2015). INGV-DPC deliverable internal report and database by G. Vannucci, P. Imprescia, and P. Gasperini (2010), "Deliverable n. 2 of the UR2.05 in the INGV-DPC S1 project (2007–2009)," was also used. The World Stress Map database release was used http://dc-app3-14.gfz-potsdam.de/ (last accessed March 2014).

Acknowledgments

We wish to thank the Aeronautica Militare Italiana for the photographic material and two anonymous reviewers for their careful reviews. We are also especially grateful to Gianluca Valensise for constructive comments and suggestions.

References

Anzidei, M., A. Maramai, and P. Montone (Editors) (2012). The Emilia (northern Italy) seismic sequence of May–June, 2012: Preliminary data and results, *Ann. Geophys.* **55,** no. 4, 843.

Bakun, W. H., and C. M. Wentworth (1997). Estimating earthquake location and magnitude from seismic intensity data, *Bull. Seismol. Soc. Am.* **87,** 1502–1521.

Bally, A. W., L. Burbi, C. Cooper, and R. Ghelardoni (1986). Balanced sections and seismic reflection profiles across the central Apennines, *Memor. Soc. Geol. Ital.* **35,** 257–310.

Barchi, M., A. De Feyter, M. B. Magnani, G. Minelli, G. Pialli, and B. M. Sotera (1998). The structural style of the Umbria-Marche fold and thrust belt, *Memor. Soc. Geol. Ital.* **52,** 557–578.

Baroux, E., N. A. Pino, G. Valensise, O. Scotti, and M. Cushing (2003). Source parameters of the 11 June 1909, Lambesc (Provence, southeastern France) earthquake: A reappraisal based on macro- seismic, seismological, and geodetic observations, *J. Geophys. Res.* **108,** no. B9, 2454, doi: 10.1029/2002JB002348.

Basili, A., G. Smriglio, and G. Valensise (1984). Procedure di determinazione ipocentrale in uso presso l'Istituto Nazionale di Geofisica, *Atti Gruppo Nazionale di Geofisica della Terra Solida* 875–884 (in Italian).

Basili, R., and S. Barba (2007). Migration and shortening rates in the northern Apennines, Italy: Implications for seismic hazard, *Terra Nova* **19,** 462–468, doi: 10.1111/j.1365-3121.2007.00772.x.

Basili, R., G. Valensise, P. Vannoli, P. Burrato, U. Fracassi, S. Mariano, M. M. Tiberti, and E. Boschi (2008). The Database of Individual Seismogenic Sources (DISS), version 3: Summarizing 20 years of research on Italy's earthquake geology, *Tectonophysics* **453,** 20–43, doi: 10.1016/j.tecto.2007.04.014.

Bernardi, F., J. Braunmiller, and D. Giardini (2005). Seismic moment from regional surface-wave amplitudes: Applications to digital and analog seismograms, *Bull. Seismol. Soc. Am.* **95,** no. 2, 408–418, doi: 10.1785/0120040048.

Bigi, G., G. Bonardi, R. Catalano, D. Cosentino, F. Lentini, M. Parotto, R. Sartori, P. Scandone, and E. Turco (Editors) (1992). Structural Model of Italy, CNR Progetto Finalizzato Geodinamica, scale 1:500,000.

Carletti, F., and P. Gasperini (2003). Lateral variations of seismic intensity attenuation in Italy, *Geophys. J. Int.* **155,** 839–856.

Coltorti, M., and T. Nanni (1987). La bassa valle del Fiume Esino: Geomorfologia, idrogeologia e neotettonica, *Boll. Soc. Geol. Ital.* **106,** 35–51, (in Italian).

Coward, M. P., M. De Donatis, S. Mazzoli, W. Paltrinieri, and F. C. Wezel (1999). Frontal part of the northern Apennines fold and thrust belt in the Romagna-Marche arc (Italy): Shallow and deep structural styles, *Tectonics* **18,** no. 3, 559–574.

Devoti, R., A. Esposito, G. Pietrantonio, A. R. Pisani, and F. Riguzzi (2011). Evidence of large scale deformation patterns from GPS data in the Italian subduction boundary, *Earth Planet. Sci. Lett.* **311,** 230–241, doi: 10.1016/j.epsl.2011.09.034.

Di Bucci, D., and S. Mazzoli (2002). Active tectonics of the northern Apennines and Adria geodynamics: New data and a discussion, *J. Geodyn.* **34,** 687–707.

Efron, B., and R. J. Tbishirani (1986). Bootstrap methods for standard errors, confidence intervals and other measures of statistical accuracy, *Stat. Sci.* **1,** 54–77.

Elmi, C., O. Nesci, D. Savelli, and G. Maltarello (1987). Depositi alluvionali terrazzati del margine adriatico appenninico centro-settentrionale: Processi geomorfologici e neotettonica, *Boll. Soc. Geol. Ital.* **106,** 717–721 (in Italian).

Fantoni, R., and R. Franciosi (2010). Tectono-sedimentary setting of the Po Plain and Adriatic foreland, *Rendiconti Fisica Accademia dei Lincei* **21,** no. 1, S197–S209, doi: 10.1007/s12210-010-0102-4.

Favali, P., F. Frugoni, D. Monna, M. L. Rainone, P. Signanini, and G. Smriglio (1995). The 1930 earthquake and the town of Senigallia (central Italy): An approach to seismic risk evaluation, *Ann. Geofisc.* **38,** no. 5–6, 679–689.

Fisher, N. I. (1993). *Statistical Analysis of Circular Data*, Cambridge University Press, Cambridge, United Kingdom, 277 pp.

Gasperini, P., F. Bernardini, G. Valensise, and E. Boschi (1999). Defining seismogenic sources from historical earthquake felt reports, *Bull. Seismol. Soc. Am.* **89,** 94–110.

Gasperini, P., B. Lolli, and G. Vannucci (2013a). Empirical calibration of local magnitude data sets versus moment magnitude in Italy, *Bull. Seismol. Soc. Am.* **103,** no. 4, 2227–2246, doi: 10.1785/0120120356.

Gasperini, P., B. Lolli, and G. Vannucci (2013b). Body wave magnitude m_b is a good proxy of moment magnitude M_w for small earthquakes (m_b <4.5–5.0), *Seismol. Res. Lett.* **84,** no. 6, 932–937, doi: 10.1785/0220130105.

Gasperini, P., B. Lolli, G. Vannucci, and E. Boschi (2012). A comparison of moment magnitude estimates for the European-Mediterranean and Italian regions, *Geophys. J. Int.* **190,** 1733–1745, doi: 10.1111/j.1365-246X.2012.05575.x.

Gasperini, P., G. Vannucci, D. Tripone, and E. Boschi (2010). The location and sizing of historical earthquakes using the attenuation of macroseismic intensity with distance, *Bull. Seismol. Soc. Am.* **100,** no. 5A, 2035–2066, doi: 10.1785/0120090330.

Guo, Z., and Y. Ogata (1997). Statistical relations between the parameters of aftershock in time, space and magnitude, *J. Geophys. Res.* **102,** 2857–2873.

Gutenberg, B., and C. F. Richter (1954). *Seismicity of the Earth and Associated Phenomena*, Second Ed., Princeton University Press, Princeton, New Jersey, 310 pp.

Hall, P. (1992). *The Bootstrap and Edgeworth Expansion*, Springer, New York, New York, 372 pp.

Kanamori, H., and D. L. Anderson (1975). Theoretical basis of some empirical relations in seismology, *Bull. Seismol. Soc. Am.* **65,** 1073–1095.

Kastelic, V., P. Vannoli, P. Burrato, U. Fracassi, M. Tiberti, and G. Valensise (2013). Seismogenic sources in the Adriatic domain, *Mar. Petrol. Geol.* **42,** 191–213, doi: 10.1016/j.marpetgeo.2012.08.002.

Kennett, B. L. N. (2005). Seismological Tables: ak135, Research School of Earth Sciences, The Australian National University, Canberra, Australia, 290 pp.

Levret, A., J. C. Backe, and M. Cushing (1994). Atlas of macroseismic maps for French earthquakes with their principal characteristics, *Nat. Hazards* **10,** 19–46.

Lolli, B., P. Gasperini, and G. Vannucci (2014). Empirical conversion between teleseismic magnitudes (m_b and M_s) and moment magnitude (M_w) at the global, Euro-Mediterranean and Italian scale, *Geophys. J. Int.* **199,** 805–828, doi: 10.1093/gji/ggu264.

Lomax, A. (2005). A reanalysis of the hypocentral location and related observations for the great 1906 California earthquake, *Bull. Seismol. Soc. Am.* **95,** 861–877, doi: 10.1785/0120040141.

Macchiavelli, C., S. Mazzoli, A. Megna, F. Saggese, S. Santini, and S. Vitale (2012). Applying the multiple unverse method to the analysis of earthquake focal mechanism data: New insights into the active stress field of Italy and surrounding regions, *Tectonophysics* **580,** 124–149, doi: 10.1016/j.tecto.2012.09.007.

Maesano, F. E., G. Toscani, P. Burrato, F. Mirabella, C. D'Ambrogi, and R. Basili (2013). Deriving thrust fault slip rates from geological modeling: Examples from the Marche coastal and offshore contraction belt, northern Apennines, Italy, *Mar. Petrol. Geol.* **42,** 122–134, doi: 10.1016/j.marpetgeo.2012.10.008.

Malinverno, A., and W. B. F. Ryan (1986). Extension in the Tyrrhenian Sea and shortening in the Apennines as result of arc migration driven by sinking of the lithosphere, *Tectonics* **5,** no. 2, 227–245.

Margottini, C., N. N. Ambraseys, and A. Screpanti (1993). *La magnitudo dei terremoti italiani del XX Secolo*, E.N.E.A. Internal Publication, Rome, Italy, 57 pp. (in Italian).

Mazzoli, S., C. Macchiavelli, and A. Ascione (2014). The 2013 Marche offshore earthquakes: New insights into the active tectonic setting of the outer northern Apennines, *J. Geol. Soc.* doi: 10.1144/jgs2013-091.

Michelini, A., B. De Simoni, A. Amato, and E. Boschi (2005). Collecting, digitizing, and distributing historical seismological data, *Eos Trans. AGU* **86,** no. 28, 261, doi: 10.1029/2005EO280002.

Mucciarelli, M. and P. Tiberi (Editors) (2007). *Scenari di pericolosità sismica della fascia costiera marchigiana. La microzonazione sismica di Senigallia*, Regione Marche-Istituto Nazionale di Geofisica e Vulcanologia, Tecnoprint srl, Ancona, 316 pp. (in Italian).

Oddone, E. (1930). Sul terremoto delle Province Ancona e Pesaro avvenuto il di 30 ottobre 1930, *Boll. Soc. Seismol. Ital.* **XXIX,** 115–140 (in Italian).

Okada, Y. (1985). Surface deformation due to shear and tensile faults in a half-space, *Bull. Seismol. Soc. Am.* **75,** 1135–1154.

Pasarić, M., B. Brizuela, L. Graziani, A. Maramai, and M. Orlić (2012). Historical tsunamis in the Adriatic Sea, *Nat. Hazards* **61,** 281–316, doi: 10.1007/s11069-011-9916-3.

Pasolini, C., D. Albarello, P. Gasperini, V. D'Amico, and B. Lolli (2008). The attenuation of seismic intensity in Italy, Part II: Modeling and validation, *Bull. Seismol. Soc. Am.* **98,** 692–708.

Pino, N. A., B. Palombo, G. Ventura, B. Perniola, and G. Ferrari (2008). Waveform modeling of historical seismograms of the 1930 Irpinia earthquake provides insight on "blind" faulting in southern Apennines (Italy), *J. Geophys. Res.* **113,** no. B05303, doi: 10.1029/2007JB005211.

Pino, N. A., A. Piatanesi, G. Valensise, and E. Boschi (2009). The 28 December 1908 Messina Straits earthquake (M_w 7.1): A great earthquake throughout a century of seismology, *Seismol. Res. Lett.* **80,** no. 2, 243–259, doi: 10.1785/gssrl.80.2.243.

Pondrelli, S., A. Morelli, G. Ekström, S. Mazza, E. Boschi, and A. M. Dziewonski (2002). European-Mediterranean regional centroid-moment tensors: 1997–2000, *Phys. Earth Planet. In.* **130,** 71–101.

Pondrelli, S., S. Salimbeni, A. Morelli, G. Ekström, L. Postpischl, G. Vannucci, and E. Boschi (2011). European-Mediterranean Regional Centroid Moment Tensor Catalog: Solutions for 2005–2008, *Phys. Earth Planet. In.* **185,** 74–81, doi: 10.1016/j.pepi.2011.01.007.

Postpischl, D. (Editor) (1985). Atlas of isoseismal maps of Italian earthquakes, *Quaderni della Ricerca Scientifica*, Progetto Finalizzato Geodinamica, Roma, Italy, 114**,** no. 2A, 166 pp., 64 plates.

Rock, N. M. S. (1988). *Numerical Geology*, Springer-Verlag, Berlin, Germany, 427 pp.

Scognamiglio, L., E. Tinti, and A. Michelini (2009). Real-time determination of seismic moment tensor for the Italian region, *Bull. Seismol. Soc. Am.* **99,** no. 4, 2223–2242, doi: 10.1785/0120080104.

Scrocca, D. (2006). Thrust front segmentation induced by differential slab retreat in the Apennines (Italy), *Terra Nova* **18,** 154–161, doi: 10.1111/j.1365-3121.2006.00675.x.

Sieberg, A. (1931). Erdebeben, in *Handbuch der Geophysik*, B. Gutenberg (Editor), Vol. 4, Gebrűder Borntraeger, Berlin, Germany, 552–554.

Stich, D., J. Batllo, R. Macia, P. Teves-Costa, and J. Morales (2005). Moment tensor inversion with single-component historical seismograms: The 1909 Benavente (Portugal) and Lambesc (France) earthquakes, *Geophys. J. Int.* **162,** 850–858, doi: 10.1111/j.1365-246X.2005.02680.x.

Valensise, G., and D. Pantosti (2001a). The investigation of potential earthquake sources in peninsular Italy: A review, *J. Seismol.* **5,** 287–306.

Valensise, G. and D. Pantosti (Editors) (2001b). Database of potential sources for earthquakes larger than M 5.5 in Italy, *Ann. Geofisc.* Supplement to vol. 44, no. 4, 180 pp., with CD–ROM.

Vannoli, P., R. Basili, and G. Valensise (2004). New geomorphic evidence for anticlinal growth driven by blind-thrust faulting along the northern Marche coastal belt (central Italy), *J. Seismol.* **8,** 297–312.

Vannoli, P., P. Burrato, U. Fracassi, and G. Valensise (2012). A fresh look at the seismotectonics of the Abruzzi (central Apennines) following the 6 April 2009 L'Aquila earthquake (M_w 6.3), *Italian J. Geosci.* **131,** no. 3, 309–329, doi: 10.3301/IJG.2012.03.

Vannoli, P., P. Burrato, and G. Valensise (2015). The seismotectonics of the Po Plain (northern Italy): Tectonic diversity in a blind faulting domain, *Pure Appl. Geophys.* **172,** no. 5, 1105–1142, doi: 10.1007/s00024-014-0873-0.

Vannucci, G., and P. Gasperini (2003). A database of revised fault plane solutions for Italy and surrounding regions, *Comput. Geosci.* **29,** 903–909.

Vannucci, G., and P. Gasperini (2004). The new release of the database of earthquake mechanisms of the Mediterranean area (EMMA Version 2), *Ann. Geophys.* **47,** 307–334.

Villaseñor, A., and E. R. Engdahl (2005). A digital hypocenter catalog for the International Seismological Summary, *Seismol. Res. Lett.* **76,** 554–559.

Wells, D. L., and K. J. Coppersmith (1994). New empirical relationships among magnitude, rapture length, rupture width, rupture area, and surface displacement, *Bull. Seismol. Soc. Am.* **84,** 974–1002.

Istituto Nazionale di Geofisica e Vulcanologia
sezione Roma 1
Via di Vigna Murata, 605
I-00143 Rome, Italy
paola.vannoli@ingv.it
fabrizio.bernardi@ingv.it
barbara.palombo@ingv.it
(P.V., F.B., B.P.)

Istituto Nazionale di Geofisica e Vulcanologia
sezione di Bologna
Via Donato Creti 12
I-40127 Bologna, Italy
gianfranco.vannucci@ingv.it
graziano.ferrari@ingv.it
(G.V., G.F.)

Manuscript received 1 September 2014;
Published Online 19 May 2015